Sedimentary Geology 325 (2015) 158–167

Sedimentology and composition of sands injected during the seismic crisis of May 2012 (Emilia, Italy): clues for source layer identification and liquefaction regime

D. Fontana[a], S. Lugli[a], S. Marchetti Dori[a], R. Caputo[b,c], M. Stefani[b]

[a] Dipartimento di Scienze Chimiche e Geologiche, Università di Modena e Reggio Emilia, via Campi 103, 41125 Modena, Italy; corresponding author: stefano.lugli@unimore.it
[b] Dipartimento di Fisica e Scienze della Terra, Università di Ferrara, Via Saragat 1, 44122 Ferrara, Italy.
[c] Research and Teaching Centre for Earthquake Geology, Tymavos, Greece.

ABSTRACT
In May 2012 widespread sand blows formed along buried channels in the eastern sector of the Po Plain (Northern Italy) as a consequence of a series of seismic events with main shocks of Mw 6.1 and 5.9. At San Carlo (Ferrara) a trench dug a few week after the earthquakes exposed sand dikes cutting through an old Reno River channel-levee system that was diverted in the 18th century and was deposited starting from the 14th century (unit A). This sequence overlies a Holocene muddy floodplain deposits and contains scattered sandy channel deposits (unit B) and a Pleistocene channel sand unit (unit C). Sands with inverse and normal grading, concave layering and vertical lamination coexisting along the dikes suggest multiple rhythmic opening and closing of the fractures that were injected and filled by a slurry of sand during the compression pulses, and emptied during the extension phase. The pulse mechanism may have lasted for several minutes and formed well stratified sand volcanoes structures that formed at the top of the fractures. Sands from dikes and from the various units show well defined compositional fields from lithoarenitic to quartz-feldspar-rich compositions. Sands from the old Reno levee and channel fill (unit A) have abundant lithic fragments derived from the erosion of Apennine sedimentary carbonate and terrigenous successions. Composition of the sand filling the dikes show clear affinities with sand layers of the old Reno River channel (Unit A) and clearly differ from any sand from deeper Holocene and Pleistocene layers (Unit B and C), which are richer in quartz and feldspar and poorer in sedimentary lithic fragments. Sorting related to sediment flux variations did not apparently affect the sand composition across the sedimentary structures. Textural and compositional data indicate that the liquefaction processes originated from a relatively shallow source consisting of channel sands located within Unit A at 6.8.to 7.5 m depth.

Keywords: Sand liquefaction, sand composition, 2012 Emilia Romagna earthquake, fluvial deposits, Po Plain.

1. Introduction

In May 2012 the eastern sector of the Po Plain (Northern Italy) was affected by two earthquakes (Mw 6.1 and 5.9; Pondrelli et al., 2012) followed by several aftershocks (up to Mw 5.1). The seismic activity was triggered along a portion of the Apennines thrust belt buried below the alluvial plain (Pieri and Groppi, 1981). The first event produced liquefaction phenomena, surface fracturing and sand ejection, in particular in the western sector of the Ferrara province (Papathanassiou et al., 2015). In this area, the liquefaction processes were concentrated along an elongated topographic ridge corresponding to an old channel of the Reno River that was active until the end of the 18th century when it was artificially diverted.
Because of the potential destruction and damage to structures and human activities, sand-boil

and liquefaction phenomena require thorough studies to assess the geotechnical conditions that may lead to their recurrence (Chang et al., 2011). Sedimentology of the liquefaction mechanisms and the selective processes acting on sand grains are, however, less commonly explored (Ricci Lucchi, 1995; Hurst et al., 2011). This is particularly interesting because, although the phenomenon is mostly limited to sands, even gravelly sediments can be susceptible to liquefaction (Chen et al., 2008). No data are available on the possible influence of the liquefaction phenomena on the composition of sediments: does the liquefied sand retain the same petrographic composition of the source layer while travelling through the fractures? Is there any selective mechanism that may shift the sediment composition when the pressurized slurry of water and sand erupts to the ground surface? These questions are particularly significant as the sand composition may be used as a tool to pinpoint the source layers, provided that sands located at different stratigraphic layers have been petrographically characterized. This applies also to old sand blows buried by other deposits and preserved in the geologic record.

Fluvial sand composition studies have a particular significance in the late Pleistocene–Holocene Po Plain, where distinct compositional fields characterize modern sands from different streams, as well as older sediments (Lugli et al., 2007; Garzanti et al., 2011). Several key petrographic components provide diagnostic features to distinguish sand bodies buried beneath the floodplain (Johnsson et al, 1991; Arribas and Tortosa, 2003; Critelli et al., 2003; Weltje and Von Eynatten, 2004: Basu et al., 2013). In this context, we analyzed the texture and petrographic composition of sands injected during the seismic events of 2012 along the paleo-Reno River channel at San Carlo (Ferrara), and sands from subsurface deposits at different depths. The aim of the research was to provide a better understanding of earthquake-induced liquefaction mechanisms using textural and petrographic parameters to identify the possible source layers of the sand blows.

2. Geological setting

The Ferrara alluvial plain area is located on the buried sector of the Northern Apennine fold-and-thrust belt, Italy, where streams flow northeastward into the Po River and the Adriatic Sea (Fig. 1). The Northern Apennines formed mainly during the Tertiary convergence between the European and the Adria plates. The plate movement consumed the interposed Tethyan oceanic crust with the formation of an accretionary prism, which during the subsequent collisional phase produced a complex orogenic wedge (Ricci Lucchi, 1986; Bettelli and De Nardo, 2001; Argnani et al., 2004). On the northern side of the Apennine chain, these units are unconformably overlain by Miocene-Pliocene and Quaternary terrigenous deposits of the Po Plain.

The Po Plain is the syntectonic sedimentary wedge filling the Pliocene-Pleistocene Apennine foredeep. The total basin infill is up to 4 km-thick, and the Quaternary deposits reach a thickness of 1.5 km. The factors controlling the architecture of the sedimentary filling (Amorosi et al., 2008) were the contrasting rates of subsidence induced by the vertical motions of the blind thrusts buried under the foredeep deposits, such as the Ferrara fold-fault system (Pieri and Groppi, 1981). This long-term effect combined with the Holocene rise of the Adriatic Sea level reduced the gradient along a west-east drainage axis. The main drainage, the Po River, was tectonically forced to shift northwards and human pressure on the forest cover since the Bronze Age produced a generalized increase in fine bedload discharge into the Apennines tributaries (Ravazzi et al., 2013). The river network continuously shifted laterally as a consequence of climate changes and local tectonic events (Fig. 1). The late evolution of the system has been successfully traced following the physical evidence of paleochannels on the alluvial plain surface, and the older sedimentary patterns are revealed by the provenance composition signals of buried Holocene channel sands which match those of the present day

rivers (Lugli et al., 2007).

3. **The recent evolution of the Reno River**

The synergic roles of fast subsidence and large sedimentary input have produced very high sedimentation rates and frequent changes in the fluvial drainage framework of the central part of the eastern Po plain (Fig. 1). The evolution of the river network can be reconstructed and dated in great detail, through the correlation of the stratigraphic sedimentological evidence with compositional data (Lugli et al., 2007) and a large amount of historical information and accurate ancient maps (e.g., Bondesan 1989; Caputo et al., 2015).

In the late Middle Ages, the Reno River was neither able to reach the Adriatic Sea nor to directly flow into the Po River, which was running about 10 km to the north of the study area. At that time the Reno River was mostly feeding a large paludal area and only at the end of the 18th century it was successfully forced to reach the sea, through an abandoned southern distributary channel of the Po River. The diversion point is located just to the southwest of the investigated site (Fig. 1). The investigated sector of the channel-levee system was already built in its present form at the beginning the 15th century and its depositional morphology is still recognizable today. It consists of a concave belt oriented SW-NE (the former channel), bordered by two marginal ridges (the levees) rising up to 4-5 m above the surrounding floodplain. The topographic gradients created by the channel-levee ridge had a major role in the coseismic liquefaction dynamics, which was emphasized by lateral spreading phenomena (Caputo et al., 2015; Papathanassiou et al., 2015).

The old Reno River channel-levee system was deposited on top of an alluvial sedimentary succession that was thoroughly investigated by boreholes, geotechnical and geognostic surveys. The shallow sequence (Calabrese et al., 2012) can be divided into three main units (A, B, C), from the top to the bottom (Fig. 2):

- unit A, Recent channel-levee unit consisting of medium sand belts (channels) and alternate fine sand-mud bodies (levees and proximal crevasse splays), spanning from the surface to about -13 m below the old channel ridge and -5 to - 6 m below the present-day floodplain; its base has been radiocarbon dated to a numerical age of 1450-1581 BP;
- unit B, Holocene paludal unit, consisting of floodplain mud and peat, with isolated channel and crevasse-splay sand bodies; this unit is 6 to 10 m-thick and was deposited starting roughly since the beginning of the Holocene;
- unit C, latest Pleistocene floodplain unit, consisting of floodplain mud and channel and levee sand bodies deposited during and following the last glacial maximum.

The earthquake shaking produced an array of fractures roughly parallel to the old river ridge that were exposed by digging a trench opened a few weeks after the main schock. The sedimentary sequence exposed in the trench (Caputo et al., 2012) belongs to the upper part of the Recent channel-levee system of the unit A and consists of four main depositional facies associations (Fig. 2):

A1) distal levee to proximal alluvial plain silts and silty clays, with graded fine-sand overbank beds, which are partially amalgamated by bioturbation, contain root structures and show pedogenetic alteration, traces of agricultural activity and ceramic fragments;

A2) proximal levee sands and sandy silts, with direct gradation and tractive lamination structures;

A3) channel sediments consisting of medium sand, showing festoon cross stratification. The sand contains argillaceous rip-up clasts, rounded armored mud balls, wood and brick fragments;

A4) channel sands slightly older than A3, that were intercepted by drilling at the base of the trench (depth 6.8-7.5 m).

The above sequence is cross cut at high angle by several dikes which represent extension fractures infilled by sands injected upward, visible along the entire trench section. Some of them reach the topographic surface and extend horizontally outside the trench for tens of meters, while others stop below the ploughed layer (about 0.5-1 m deep); the latter has been associated with the 1570 Ferrara earthquake (Caputo et al., 2012).

4. Materials and methods

The sampling of sand has been done in a trench dug immediately after the seismic event, which allowed the detailed observation of the fluvial sedimentary sequence across the Reno River down to the depth of about 7 m (Fig. 2). The sediments consist of cross-bedded sands from the paleo-channel of the Reno River and the laminated sand-mud leeve deposits cut by the liquefaction sand dikes. We also sampled cores from deeper sand horizons crossed by drillings down to the maximum depth of 50 m. A total of 41 sand samples was collected and analyzed: 17 samples from the five dikes (named D 3, 4, 5, 6 and 7 in the trench section shown in Fig. 2), each dike sampled at different depths; 4 samples from the modern sands of the present-day Reno River; 10 samples from the levee (unit A1-A2) and channel fill (A3) of the paleo Reno River; 4 samples from paleo-channel sands drilled at the bottom of the trench (unit A4), 6 samples from cores outside the trench from unit B (borehole S2, 8.20 to10.45 m depth and borehole S3, 6.90 to 9.60 m depth) and the lower sand layer dating back to the uppermost Pleistocene (borehole S10, 22.50 to 24.50 m depth, unit C). Sample locations are shown in Fig. 2.

Grain-size analyses were performed using standard techniques: mechanical sieving for the sandy fraction and hydrometer analysis for fine-grained sediments. Sand samples consisting of a few hundreds of grams were washed with dilute H_2O_2 to remove organic matter and were air dried and mechanically sieved for granulometric and compositonal analyses. The result of grain size analyses for most of the samples is a mean value of multiple bands that are a few millimeters to centimeters in thickness, as sampling encompassed many of these vertical features (see sedimentological description).

For the compositional analyses, two sub-samples were prepared for each samples: the whole sandy fraction (for qualitative observations) and the fine sand fraction (0.125–0.250 mm) for point counting. The necessity to analyze the fine sand fraction was dictated by the lack of medium-coarse sand at some of the sampling sites and for comparison with the same grain-size fraction used in Lugli et al. (2007). Sands were impregnated in epoxy resin under vacuum, thin-sectioned, and stained for carbonate identification. Sand composition data were obtained according to the Gazzi-Dickinson method, which was designed to reduce the effect of grain size over composition (Zuffa, 1985; Weltje, 2002). Point counting under transmitted light microscopy was performed on the 0.125–0.250 mm fraction. At least 300 grains were point counted for each section to achieve modal composition (see supplementary data for complete composition data set). Components not related to the original sand composition, such as authigenic carbonate nodules, penecontemporaneous shell fragments, soil and organic fragments were excluded from the final calculations.

5. Results

5.1 Sedimentology of the sand blows

The seismically induced sand dikes represent vertical straight, planar or curved extension features crosscutting the sequence at high angles from the base of the trench to the

topographic surface with a vertical extension of at least 5 m. In several cases (dikes D 5, 6, 7) they stop 1 m or a few decimetres below the surface, but the main fracture may have reached the surface elsewhere. The width of the fractures varies from a few centimetres to about 30 cm. Most fractures are single, but bifurcations are also present; some show tapering (Figs. 3, 4). Some fracture margins are closely spaced locally and are partially filled by muddy fragments from the host sediment (Fig. 3).
The sand injected into the fractures shows complex sedimentary structures similar to those described by Nichols et al. (1994), Ricci Lucchi (1995) and Hurst et al. (2011; see also references therein). The most common feature is a distinct banding, that ranges in thickness from 0.3 to 3 cm (Fig. 5), and can be longitudinal to the dike length, or perpendicular to the dike margins (Figs. 3-5). The bands oriented parallel to the dike are bounded by sharp contacts marked by thin clay veneers and are defined by differences in grain size and grain alignment. The multiple sets of graded layers that form the banding may show variable thickness along the dikes and some bands scoured into adjacent layers (Figs. 3, 4). The largest fractures are filled by sand graded along the vertical fissures (Fig. 5), and show an internal stratification consisting of multiple superimposed concave fine-grained veneers (Fig. 3). We observed both normal and inverse vertical grading of the sand from medium sand to mud. Similar well-laminated structures are observed in sand volcanoes that formed on the top of the fractures in many of the liquefaction sites around San Carlo (Fig. 6).

5.2 Grain-size distribution

Results of grains size analysis are reported in Figure 7. The content of sand, silt and clay for all samples is shown in the triangular plot of Figure 8. The samples range from almost pure sands to silt, with a content of clay less than 20%. Samples from the levee facies are the finest, made up of coarse silt to very fine to fine sands. Samples from the paleo-channel and from deeper layers are predominantly medium and medium-coarse sands. The dikes consist mainly of very fine to fine and medium sands. In four samples the amounts of coarse sand is higher than 10 %. One dike sample is made up of silt. In all dikes the amount of clay is less than 10 %. The grain-size distribution along the same dike shows no systematic trends, as samples located nearby each other may have different grain size. This is shown by the diagram of Fig 9 that plots the mean diameter for each dike at different depth: dike D 3 is characterized by a slight grain size increase from the lower portion to the top, while an opposite trend is observed in dike 5. Sorting of all sands is moderate to poor and for the dikes ranges from 1.22 to 2.46 phi.

5.3 Sand composition

5.3.1 The modern Reno River fluvial sands.
Among the examined samples, the sands from the modern Reno River are the most lithoarenitic; they are made up of quartz (ranging from 29.7 to 35.2%.), feldspars (15.2-21.7%) and sedimentary fine-grained siliciclastic and carbonate lithics. Shales are the dominant lithic grains (12.4-18.6%); they are well lithified, well rounded, with an evident iso-orientation of clay minerals, and for these characters they appear to have a detrital origin, derived from older pelitic successions of the Northern Apennines. Minor intrabasinal muddy components consisting of penecontemporaneous rip-up clasts have also been observed. Sands of the modern Reno River are well distinguishable from the other rivers of the Po Plain, as defined by Lugli et al. (2007).

5.3.2 The paleo Reno River fluvial sands

The sand samples from the paleo-Reno levee (unit A1-A2) and channel fill (A3) are quite homogeneous in composition (Fig. 10 a, b), slightly impoverished in lithic fragments compared to the modern Reno River sands. The amount of quartz ranges from 29.7 to 37.7%. Feldspars (both plagioclase and K-feldspar) vary from 18.1 to 23.7%. Fine-grained lithics are mainly sedimentary, made up of micritic and sparitic limestones (from 9.4 to 17.0%) and siltstones and shale (14.4 to 20.4%). Metamorphic lithics and cherts are minor components.

The composition of older channel sands (Unit A4), shows quartz content ranging from 28,8 to 39.6%, feldspars from 20.1 to 26.6%, siltstones and shale vary from 14.5 to 23%, carbonates from 21.3 to 23.7%.

5.3.3 The sand dikes

The sands filling the dikes show relatively homogeneous composition (Fig. 10c) with one exception. Total quartz range from 31.2 to 42.2%, feldspars from 16.3 to 24.9%. Carbonate lithics vary from 22.3 to 30.2%; siltstones and shales range from 11.8 to 18.4%. Only one sample (no. 23) from the deepest portion of dike 3, shows higher quartz and feldspar content and is very low in siliciclastic lithics. Sands from single dikes at different depths show minor, non-systematic, compositional variations, mainly due to quartz and lithic fragments variations (see Fig. 9).

5.3.4 The older sands: Holocene (unit B) to Pleistocene (unit C)

The core fluvial sands in the subsurface at depths from 7 to 10 m (Holocene) and from 22 to 24 m (Pleistocene in age) are rich in quartz and feldspar and metamorphic rock fragments (Fig.10d). Quartz range from 36.7 to 54.0%; feldspars vary from 19.7 to 28.6%; siltstones and shales are less than 11% and carbonate lithics range from 16 to 29.1%. Coarse-grained metamorphic rock fragments are also present.

5.3.5 Compositional fields

Data from modal analyses are reported in the ternary diagram Q+F (quartz+feldspars), L (silicicclastic fine-grained lithics), C (carbonate lithics) of Fig. 11, in which compositional fields of others fluvial sands in the Po Plain are also reported (Lugli et al., 2007).

The examined sands are characterized by well defined fields and show a clear trend from lithoarenitic to quartz-feldspar-rich compositions. In detail the sands from the modern Reno River are the most lithoarenitic, with shales as the dominant lithic type. Sands are well distinguishable from the other rivers of the Po plain, as defined by Lugli et al. (2007). The sands from the paleo-Reno channel fill are slightly enriched in quartz and feldspars and impoverished in lithic fragments compared to the modern Reno River sands. A composition similar to the paleo-Reno channel fill characterizes also sands at shallow depth (unit A4, 6.8-7.5 m depth). In the modern and paleo Reno river sands the lithic fragments derive mostly from the erosion of sedimentary carbonate and terrigenous Mesozoic and Cenozoic Apennine successions.

Composition of dike sands clearly overlap that of the paleo-Reno river sands down to the depth of 7.5 m. Older Holocene sands coming from layers deeper than 8 m and the Pleistocenic sands (unit C) differ in composition and show an higher quartz-feldspar content.

A similar enrichment in quartz and feldspars in the Pleistocene fluvial sands, compared with the present-day sands, was noted by Lugli et al. (2007) for the fluvial sediments of the Po alluvial plain. This shifting composition back in time was interpreted as a consequence of the different climatic weathering condition that occurred during the last glacial stage. The strong denudation, erosion and accelerated transport were probably responsible of promoting the survival of the feldspar grains.

5.3.6 Grain-size influence on sand composition

As the counting technique here adopted (Zuffa, 1985) is especially designed to minimize the dependence of the analysis from the grain-size. We plotted the mean diameter and the percentage of significant types of grains (quartz and feldpars, shales, carbonates) in order to verify the reliability of the point counting analyses. Figure 12 shows no correlation between composition and grain-size of sands. These results suggest that disintegration, microfracturing or erosion of most erodible grains, such as shales, due to the abrasive flow of sand grains was not responsible of significant compositional variation.

6. Discussion

In our study, texture and composition characteristics provide important constrains for source layer identification in liquefaction processes and flow regime.

Although there is currently no unequivocal evidence that grain texture in sand dikes (i.e., lamination, clay content, alignment of platy and elongate grains) may be indicative of a particular flow regime (Hurst et al., 2011), the diverse sedimentary features coexisting within the same dike, are probably related to the multiple rhythmic opening and closing of the fracture boundaries that may have lasted for several seconds or minutes. The sedimentary features suggest that the fractures were rhythmically injected and filled of slurry sand and mud during the compression pulses, and emptied by the rushing of the slurry back down deep into the fractures during the extension peak. These alternate flows, together with the sequential opening of various fractures in the area, may account for the presence of both inverse and normal grading of the sand filling different portions of the same dike, and for the concave-shaped layering of the dikes. Unfortunately this phenomenon was not observed directly in May 2012, but similar examples, although of much larger magnitude, were filmed during the Mw 9.0 Tohoku great earthquake in Japan (see Great Japan Earthquake, 2011, www.youtube.com/watch?v=TzlodnjPAuc).

The pulse mechanism of sand blows is also supported by the well stratified structure of the sand volcanoes that formed on the top of the fractures in many of the liquefaction sites around San Carlo (Fig. 6) and elsewhere, a feature described also by Rodríguez-Pascua et al. (2015). These volcanoes are up to a few tens of centimeters high and show alternate cm-mm scale graded laminae consisting of sand and mud (Fig. 6).

The grain-size distribution of the sands filling dikes clearly overlaps that of sands at depths of 6.8-7.5 meters, and in deeper layers. The grain-size distribution of examined dikes show a good agreement with the grain-size characteristic reported in the literature for sands ejected during earthquakes in California and Japan (Kishida, 1970; Figueroa et al., 1995). In particular, the amount of clay (less than 10%) fits with other case histories that show that only sand with a low natural clay content are susceptible to liquefaction. Tokimatsu and Yoshimi (1983) documented 70 cases in Japan resulting from 10 separate earthquakes that show a cut-off for liquefaction susceptibility at a clay content of about 15-10%.

The composition adds an important constraint in identifying the source layer. Composition of the sand filling the dikes shows close similarity with the composition of the sand layer located at a depth from 6.8 to 7.5 metres (Unit A4), and clearly differs from deeper sands which are richer in quartz and feldspar and poorer in sedimentary lithic fragments. These data clearly indicate a relatively shallow source for the blowouts. It is known that the liquefaction resistance of a soil deposit increases with depth as the effective overburden pressure increases and for this reason, sand deposits deeper than about 15 m are rarely observed to liquefy (Krinitzsky et al., 1988). Particle cementation, not observed in the examined dike sands, is also an important factors and layers older than the Holocene are usually not prone to liquefaction (Youd and Perkins, 1978), perhaps due to a weak cementation of the grains.

Our data seem to indicate that no major compositional variations were induced by grain size selective mechanism due to flux variation for liquefaction phenomena.
Finally, an interesting point concerns the enrichment in quartz and feldspars in the relatively shallow sands of unit B deposited by the Reno River in the Holocene (pre 16th century), which are similar to the deeper Pleistocene sands (unit C). This could be due to partial recycling of sands deposited during the last glacial maximum at about 20 ka. Another possibility is that the drainage network was different from that of today, as suggested by Ravazzi et al. (2013), and that the sand may have been deposited by another river, the Enza, which is today flowing much farther to the west than the Reno River.

6. Conclusions

- The study of the sands injected in the San Carlo area (Ferrara) during the Mw 6.1 earthquake, and the comparison of their texture and composition with those of buried fluvial sediments as deep as 20 m provided us with clues about the emplacement mechanisms and the source layers of injected sands.
- The sands from the dikes show a composition compatible with that of the recent shallow sands deposited by the Reno River. These sands clearly differ from deeper sands (at depth of more than 8 m). The former are richer in quartz and feldspar and poorer in sedimentary lithic fragments as a consequence of their deposition during the last glacial maximum and later reworking.
- Composition and fabric characteristics, such as grain-size distribution and clay content, indicate that liquefaction processes affected mainly sand layers at depth of 6.8-7.5 m, a relatively shallow source for the blowouts. Pulsations in the flow during shaking appear to be responsible for the vertical layering within the dikes, normal and inverse gradation along the dikes and only modest petrographic compositional variations within individual dikes.
- Our results show that grain size selective mechanisms have not influenced the sand composition and thus petrographic point-counting methodology may be successfully applied to trace back the source sand layers of ancient blowouts.

Acknowledgements
We thank the two anonymous reviewers for constructive comments that improved the manuscript. We are indebted to the Municipality of Sant'Agostino and Regione Emilia Romagna for supporting the trench investigation and core sampling. We thank D. Castaldini, G. Bertolini, C. Fioroni and M. Bertacchini for their help in sampling, and E. Carnevali for grain size analyses.

References

Amorosi, A., Pavesi, M., Ricci Lucchi, M., Sarti, G., Piccin, A., 2008. Climatic signature of cyclic fluvial architecture from the Quaternary of the central Po Plain, Italy. Sedimentary Geology 209, 58–68.

Argnani, A., Fontana, D., Stefani, C., Zuffa, G.G., 2004. Late Cretaceous carbonate turbidites of the northern Apennines: Shaking Adria at the onset of Alpine collision. Journal of Geology 112, 251-259.

Arribas, J., Tortosa, A., 2003. Detrital modes in sedimenticlastic sands from first-order streams of the Iberian Range, Spain: The potential for sand generation of different sedimentary rocks. Sedimentary Geology 159, 275- 303.

Bettelli, G., De Nardo, M.T., 2001. Geological outlines of Emilia Apennines (Italy) and introduction to the rock units cropping out in the areas of landslides reactivated in the 1994–1999 period. Quaderni di Geologia Applicata 8, 7–26.

Bondesan, M.,1989. Evoluzione geomorfologica e idrograficadella pianura ferrarese. Terre ed Acqua, Corbo Editore, 14-20.

Basu, A., Schieber, J., Patranabis–Deb, S., Chandra Dhang, P., 2013. Recycled detrital quartz grains are sedimentary rock fragments indicating unconformities: examples from the Chhattisgarh Supergroup, Bastar craton, India. Journal of Sedimentary Research 83, 368–376.

Burrato, P., Vannoli, P., Fracassi, U., Basili, R., Valensise, G., 2012. Is blind faulting truly invisible? Tectonic-controlled drainage evolution in the epicentral area of the May 2012, Emilia-Romagna earthquake sequence (northern Italy). Annals of Geophysics 55, 525–531

Calabrese, L., Martelli, L., Severi, P., 2012. Stratigrafia dell'area interessata dai fenomeni di liquefazione durante il terremoto dell'Emilia (maggio 2012). 31° Conv. Naz. GNGTS, Potenza, November 2012, 2, 119–126.

Caputo, R., Iordanidou, K., Minarelli, L., Papathanassiou, G., Poli, M.E., Rapti-Caputo, D., Sboras, S., Stefani, M., Zanferrari, A., 2012. Geological evidence of pre-2012 seismic events, Emilia-Romagna, Italy. Annals of Geophysics 55, 743-749.

Caputo, R., Pellegrinelli, A., Bignami, C., Bondesan, A., Mantovani, A., Stramondod, S., Russo, P., 2015. High-precision levelling, DInSAR and geomorphological effects in the Emilia 2012 epicentral area. Geomorphology 235, 106–117

Chang, W.-J., Ni., S.-H., Huang, A.-B., Huang, Y.-H., Yang, Y.-Z., 2011. Geotechnical reconnaissance and liquefaction analyses of a liquefaction site with silty fine sand in Southern Taiwan. Engineering Geology 123, 235–245.

Chen, L., Hou, L., Cao, Z., Yuan, X., Sun, R., Wang, W., Mang, F., Chen, H., Dong, L., 2008. Liquefaction investigation of Wenchuan earthquake. Paper no. S31-049 The 14th World Conference on Earthquake Engineering, October 12-17, 2008, Beijing, China.

Critelli, S., Arribas, J., Le Pera, E., Tortosa, A., Marmaglia, K.M., Latter, K.K., 2003. The recycled orogenic sand provenance from an uplifted thrust belt, Betic Cordillera, southern Spain. Journal of Sedimentary Research 73, 72–81.

Figueroa, J.L., Saada, A.S., Liang, L., 1995. Effect of the Grain Size on the Energy Per Unit Volume at the Onset of Liquefaction. Proceedings: 3rd International Conference on Recent Advances in Geotechnical Earthquake Engineering and Soil Dynamics 1, 197-202

Garzanti, E., Vezzoli, G., Andò, S., 2011. Paleogeographic and paleodrainage changes during Pleistocene glaciations (Po Plain, Northern Italy). Earth Science Reviews 105, 25-48.

Hurst, A., Scott, A., Vigorito, M., 2011. Physical characteristics of sand injectites. Earth-Science Reviews 106, 215–246.

Johnsson, M.J., Stallard, R.F., and Lundberg, N., 1991. Controls on the composition of fluvial sands from a tropical weathering environment; sands of the Orinoco River drainage basin, Venezuela and Colombia. Geological Society of America Bulletin 103, 1622–1647.

Kishida, H., 1970. Characteristics of Liquefaction of Level Sandy Ground During the Tokachioki Earthquake. Soils and Foundations 10, 103-111.

Krinitzsky, E. L., Chang, F. K., Nuttli, O. W. 1988. Magnitude-related earthquake ground motions. Bulletin of the Association of Engineering Geologists XXV, 399–423.

Lugli S., Marchetti Dori S., Fontana D. 2007. Alluvial sand composition as a tool to unravel the Late Quaternary sedimentation of the Modena Plain, northern Italy. In: Arribas, J., Critelli, S., Johnsson, M.J. (Eds.), Sedimentary Provenance and Petrogenesis: Perspectives from Petrography and Geochemistry. Geological Society of America Special Paper 420, pp. 57-72.

Nichols, R.J., Sparks, R.S.J., Wilson, C.J.N., 1994. Experimental studies of the fluidization of layered sediments and the formation of fluid escape structures. Sedimentology 41, 233-253.

Papathanassiou, G., Mantovani, A., Tarabusi, G., Rapti, D., Caputo, R., 2015. Assessment of liquefaction potential for two liquefaction prone area considering the May 20, 2012 Emilia (Italy) earthquake. Engineering Geology 189, 1-16.

Pieri, M., Groppi, G., 1981. Subsurface geological structure of the Po Plain, Italy. C.N.R., Progetto Finalizzato Geodinamica 414, 1-13.

Pondrelli, S., Salimbeni, S., Perfetti, P., Danecek, P., 2012. Quick regional centroid moment tensor solutions for the Emilia 2012 (northern Italy) seismic sequence. Annals of Geophysics 55, 615-621.

Ravazzi, C., Marchetti, M., Zanona, M., Peregoc, R., Quirino, T., Deaddis, M., De Amicis, M., Margaritora, D., 2013. Lake evolution and landscape history in the lower Mincio River valley, unravelling drainage changes in the central Po Plain (N-Italy) since the Bronze Age. Quaternary International 288, 195-205.

Ricci Lucchi F., 1986. Oligocene to Recent foreland basins Northern Apennines. In: Allen, P.A., Homewood, P. (Eds), Foreland basins, I.A.S. Special Publicication, Oxford Blackwell Scientific 8, 105-139.

Ricci Lucchi F., 1995. Sedimentological indicators of paleoseismicity. In: Serva, L., Slemmons, D.B. (Eds.), Perspective in paleosismology, Association for Engineering Geology, Special Publication 6, 7-18.

Rodríguez-Pascua, M.A., Pablo G. Silva, P.G., Perez-Lopez, R., Giner-Robles, J.L., Martín-Gonzalez, F., Del Moral, B., 2015. Polygenetic sand volcanoes: On the features of liquefaction processes generated by a single event (2012 Emilia Romagna 5.9 Mw earthquake Italy). Quaternary International 357, 329-335.

Tokimatsu., K., Yoshimi, Y., 1983. Empirical Correlation of Soil Liquefaction Based on SPT N-Values and Fines Content. Soils and Foundations 23, 56-74.

Weltje, G.J., 2002. Quantitative analysis of detrital modes: Statistically rigorous confidence regions in ternary diagrams and their use in sedimentary petrology. Earth-Science Reviews 57, 211–253.

Weltje, G.J., Von Eynatten, H., 2004. Quantitative provenance analysis of Sediments. Review and outlook. Sedimentary Geology 171, 1–11.

Youd, T.L., Perkings, D.M., 1978. Mapping liquefaction induced ground failure potential. Journal of the Geotechnical Engennering Division 104, 443-446.

Zuffa, G.G., 1985. Optical analyses of arenites: Influence of methodology on compositional results. In: Zuffa, G. (Ed.), Provenance of Arenites. Dordrecht/Boston/Lancaster, D. Reidel Publishing Company, NATO ASI 148, pp.165–189.

Figure captions

Fig. 1. Sketch map of the alluvial plain in the Emilia area affected by the May 2012 earthquakes (location of the two major epicenters are indicated with stars). The studied trench is located at San Carlo, along an old Reno River channel abandoned as a result of the 18th century diversion. Arrows indicate the river channel shift trends during the Holocene (modified from Burrato et al., 2012).

Fig. 2. a) Stratigraphic section of the old Reno river channel ridge at San Carlo. Depositional facies and stratigraphic units (modified after Caputo et al. 2012; Papathanassiou et al., 2015). b) Stratigraphy and depositional units in the trench exposure along two walls (upper section flipped) showing the sand dikes cutting the fluvial sequence. Sample location is also reported. (modified after Caputo et al., 2012)

Fig. 3. Dike D7 filled by laminated sand cutting through stratified proximal levee sand and silt facies. The left side of the wall collapsed as a result of lateral spreading. Laminae within the dike are highlighted by concave silt veneers suggesting multiple phases of sediment settling by collapse of the sand column along the fracture. The fracture is locally filled by silty clast originated by the mechanical crushing of the fracture borders (upper right). Location of dike in the trench is shown in Figure 2.

Fig. 4. Dike D5 cutting across bioturbated massive clayey silt. Note the cross cutting relationships between the larger and smaller fracture which are also marked by a few oblique fine-grained laminae (upper left). Sand in the larger dike is normally graded. Location of dike in the trench is shown in Figure 2.

Fig. 5. Distinct vertical lamination within dike D3. Single sand layers are graded and are separated by thin fine-grained laminae. Layering is accentuated by differential weathering. Location of dike in the trench is shown in Figure 2.

Fig. 6. Ejected sand at San Carlo forming a volcano structure consisting of various laminated sand layers. At least 6 sand/mud couplets are visible indicating variations in sediment/water volumes, possibly due to multiple opening and closing phases of the mother fracture.

Fig. 7. Cumulative grain size distributions of sands from the paleo Reno River levee and channels, cores from units B and C, and the dikes.

Fig. 8. Triangular plot showing the relative proportions of sand, silt and clay for the examined samples.

Fig. 9. Variations in grain size (mean diameter), quartz+feldspars and shale contents in a vertical profile along dikes 3 and 5.

Fig. 10. Photomicrographs of sands from the old Reno River (a) channel, (b) levee, (c) dike D3 and (d) Pleistocene sands of unit C. Transmitted light, crossed polars. Cal = calcite spar; Q = quartz; F = feldspar; Sh = shale.

Fig. 11. Q+F, L, C diagram showing the composition of sands from dikes, recent and paleo Reno River and from older units B and C. Composition of sands from the Modena plain streams is also reported (Lugli et al., 2007). Q: quartz; F: feldspars; L: siliciclastic rock fragments; C: carbonate rock fragments.

Fig. 12 Plot showing the content of quartz+ feldspar vs the mean diameter for all the examined samples. Note the lack of correlation between grain-size and composition. This result is confirmed for the other compositional classes (not reported here).

SUPPLEMENTARY DATA

Table 1. Results of petrographic modal analyses.

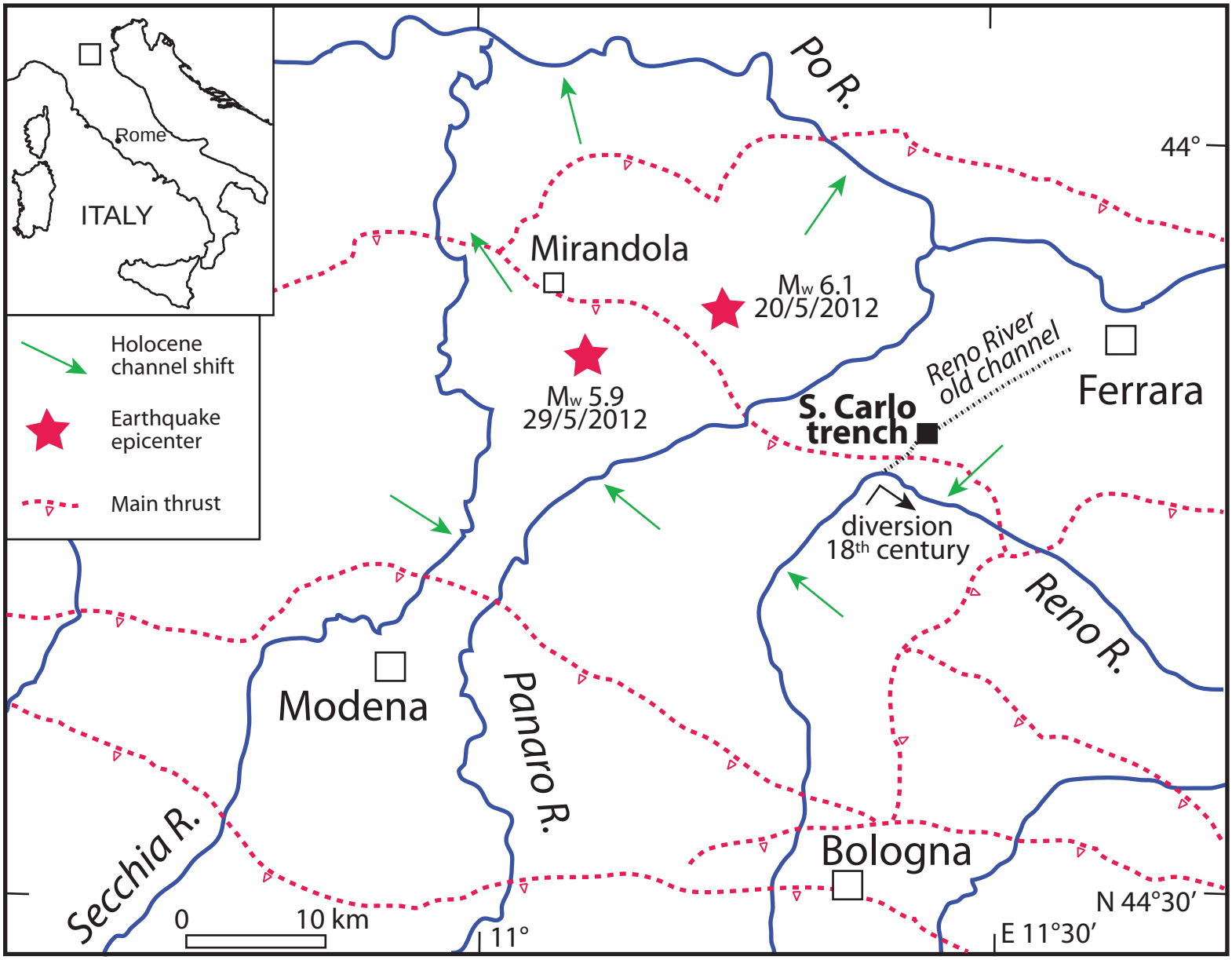
Rome
ITALY
Holocene channel shift
Earthquake epicenter
Main thrust
Po R.
44°
Mirandola
Mw 6.1
20/5/2012
Mw 5.9
29/5/2012
Reno River old channel
Ferrara
S. Carlo trench
diversion
18th century
Reno R.
Modena
Panaro R.
Secchia R.
Bologna
0
10 km
11°
N 44°30′
E 11°30′

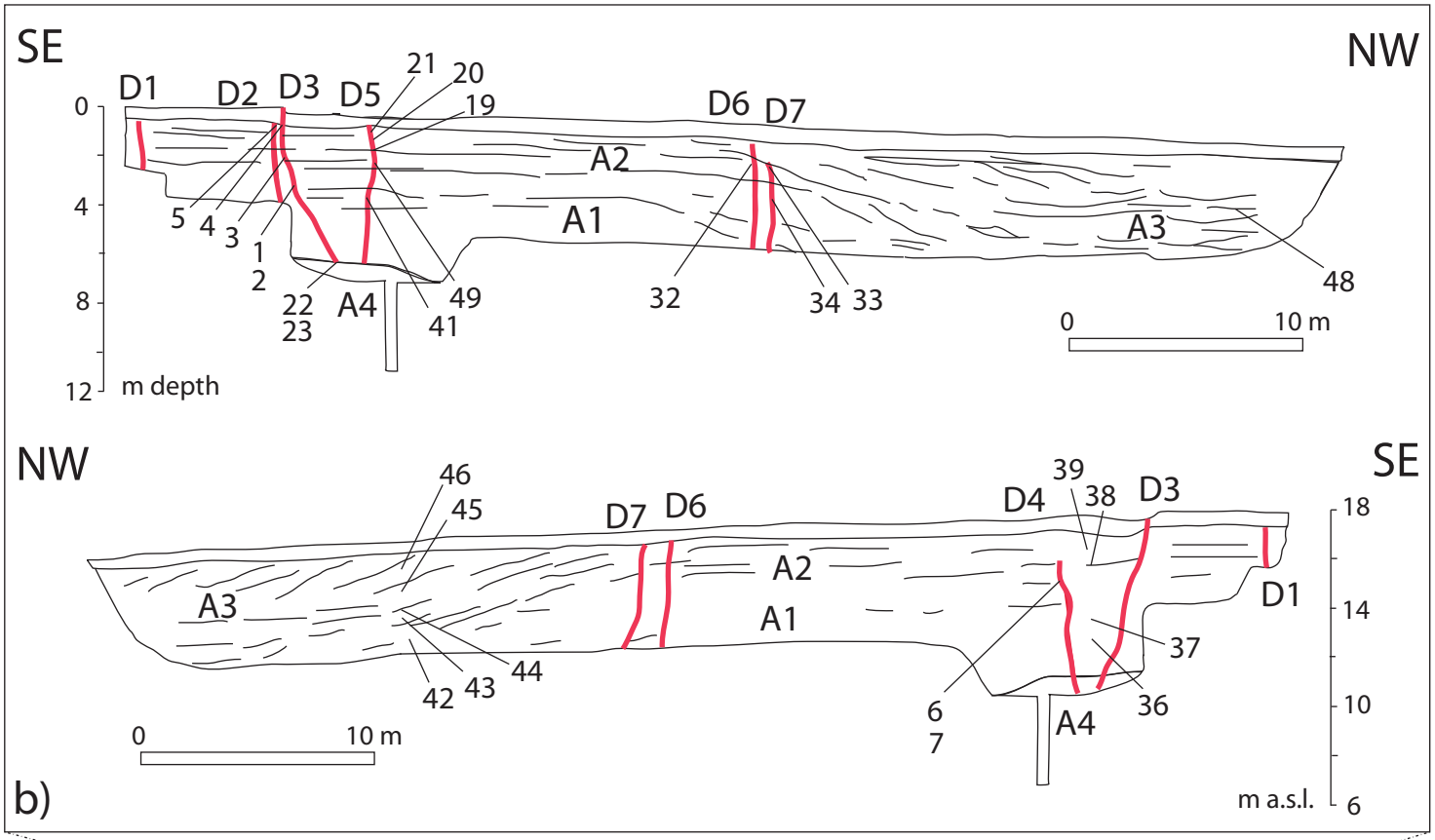
SE
NW
D1
D2
D3
D5
21
20
19
D6
D7
A2
A1
A3
5
4
3
1
2
22
23
A4
49
41
32
34
33
48
0
4
8
12
m depth
0
10 m
NW
SE
46
45
D7
D6
39
38
D4
D3
A2
A1
A3
D1
37
36
6
7
A4
42
43
44
0
10 m
18
14
10
6
m a.s.l.
b)

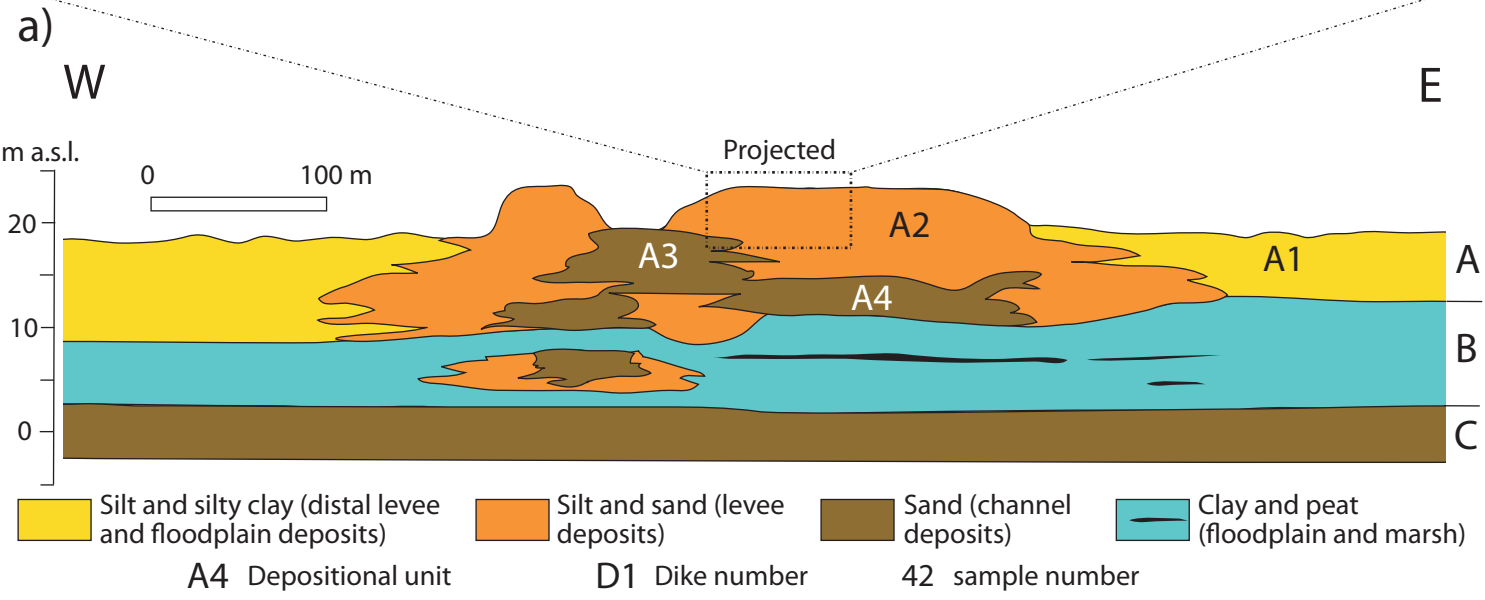
a)
W
E
m a.s.l.
0
100 m
Projected
20
10
0
A2
A3
A1
A4
A
B
C
Silt and silty clay (distal levee and floodplain deposits)
Silt and sand (levee deposits)
Sand (channel deposits)
Clay and peat (floodplain and marsh)
A4 Depositional unit
D1 Dike number
42 sample number

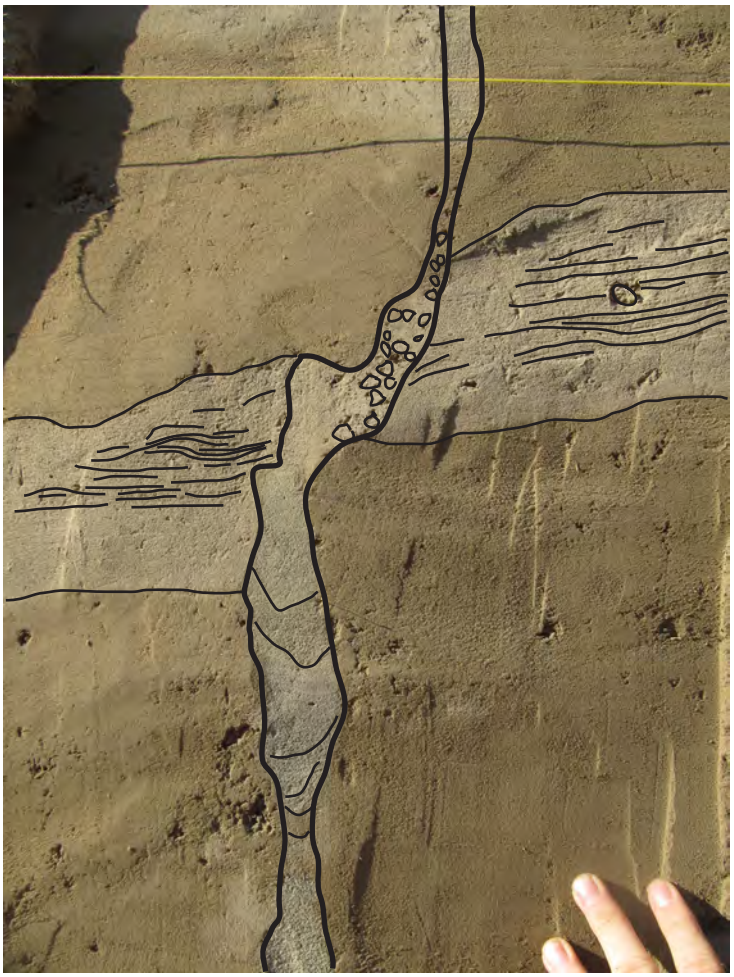


0

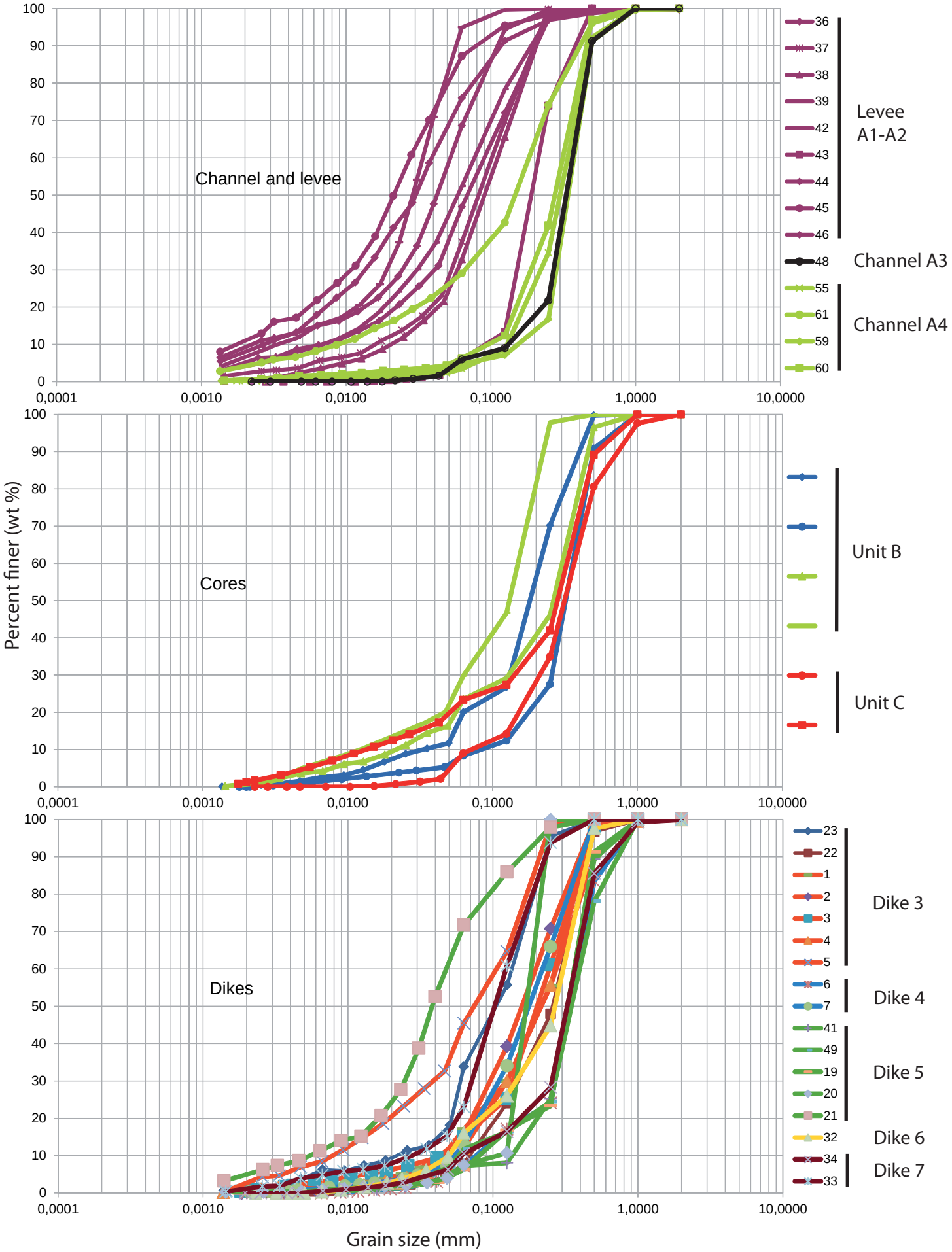
Channel and levee
Cores
Dikes
Percent finer (wt %)
Grain size (mm)
0,0001
0,0010
0,0100
0,1000
1,0000
10,0000
0
10
20
30
40
50
60
70
80
90
100
36
37
38
39
42
43
44
45
46
48
55
61
59
60
Levee A1-A2
Channel A3
Channel A4
Unit B
Unit C
23
22
1
2
3
4
5
6
7
41
49
19
20
21
32
34
33
Dike 3
Dike 4
Dike 5
Dike 6
Dike 7

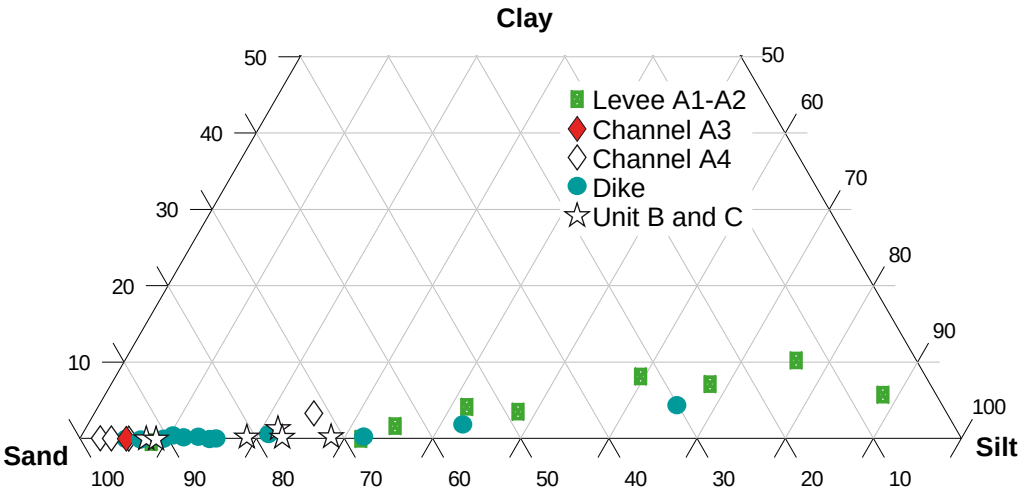
Clay
Sand
Silt
50
40
30
20
10
60
70
80
90
100
Levee A1-A2
Channel A3
Channel A4
Dike
Unit B and C

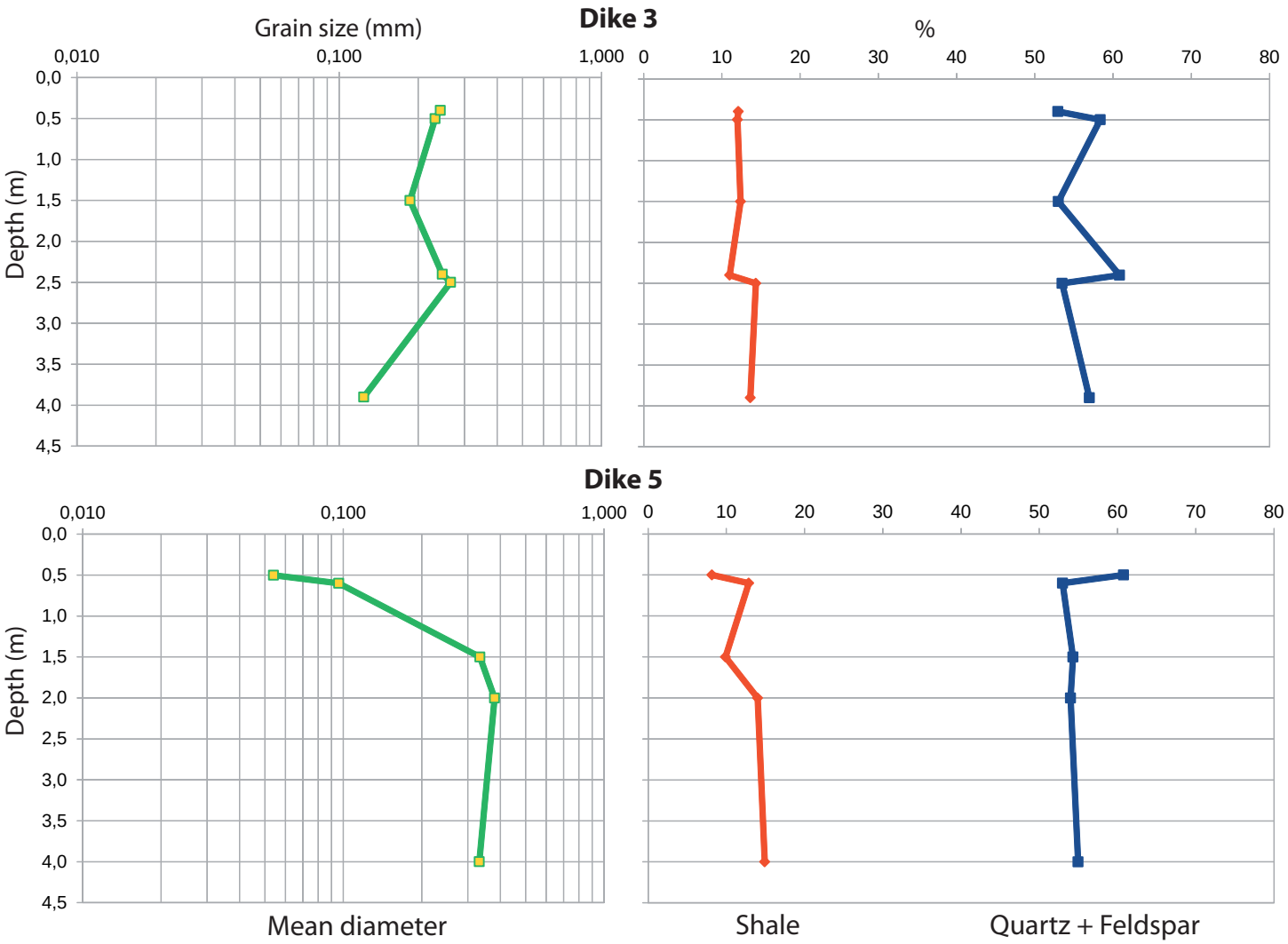
Dike 3
Grain size (mm)
0,010
0,100
1,000
%
0
10
20
30
40
50
60
70
80
Depth (m)
0,0
0,5
1,0
1,5
2,0
2,5
3,0
3,5
4,0
4,5
Dike 5
Mean diameter
Shale
Quartz + Feldspar

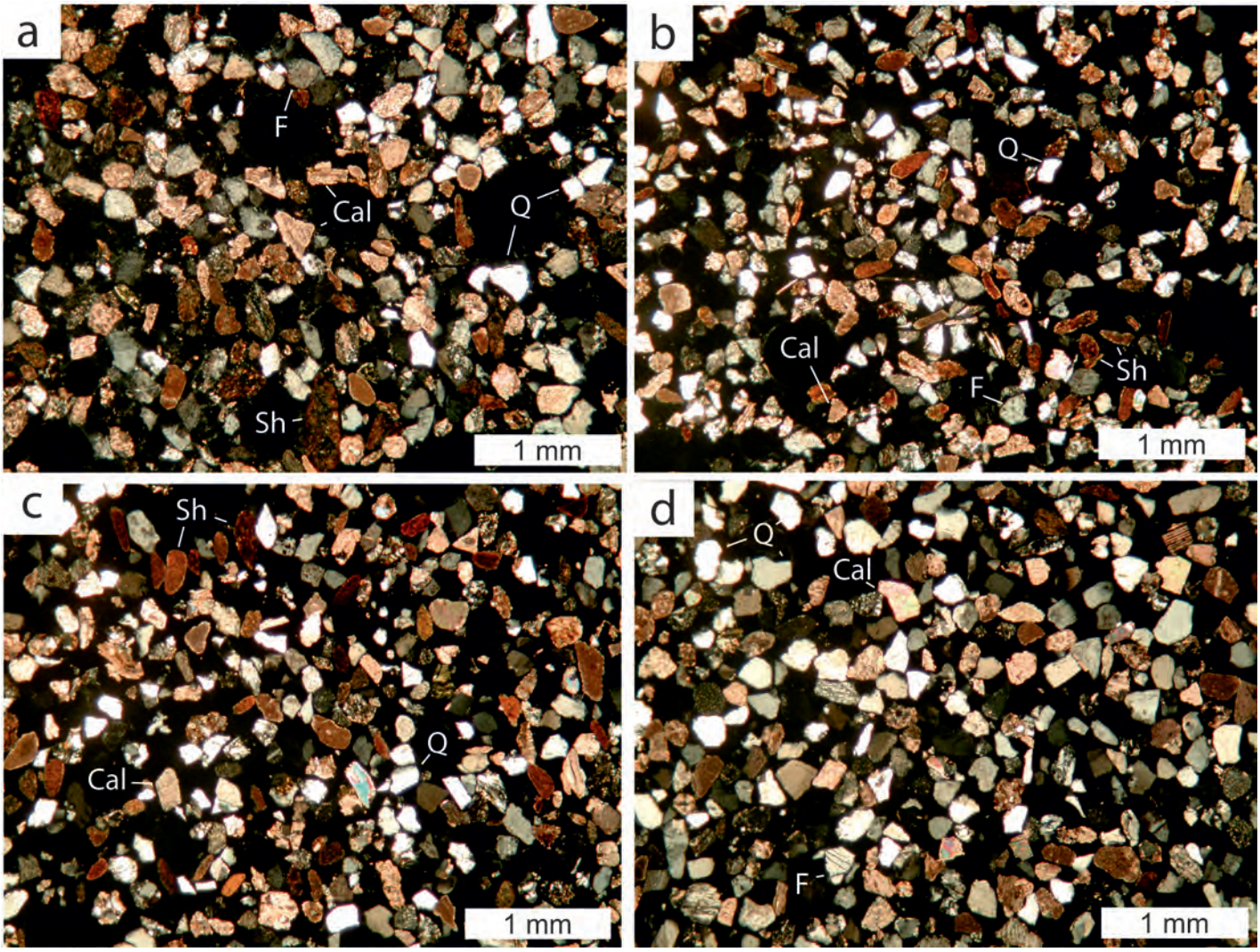
a
F
Cal
Q
Sh
1 mm
b
Q
Cal
F
Sh
1 mm
c
Sh
Q
Cal
1 mm
d
Q
Cal
F
1 mm

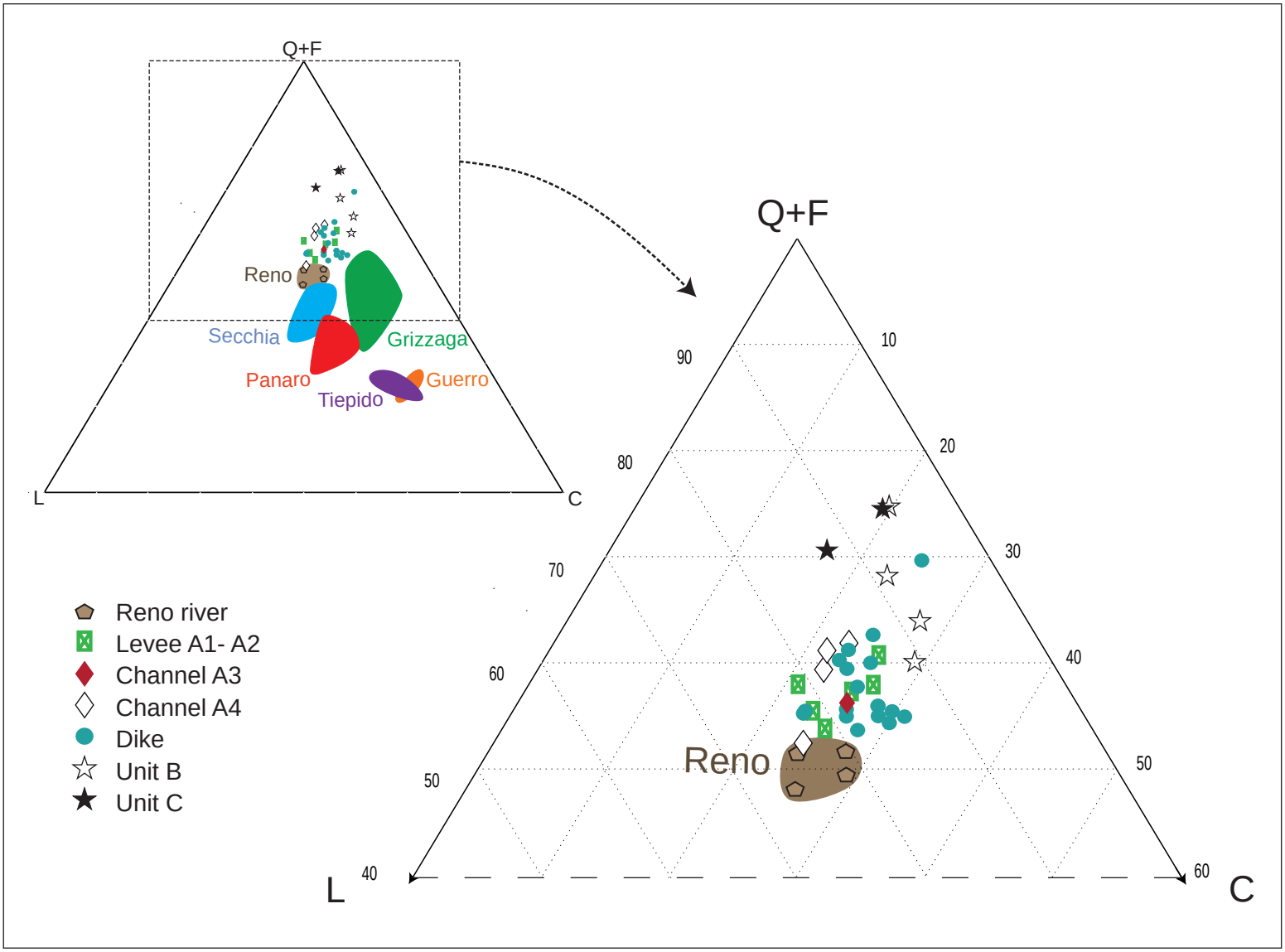
Q+F
Reno
Secchia
Grizzaga
Panaro
Guerro
Tiepido
L
C
Reno river
Levee A1- A2
Channel A3
Channel A4
Dike
Unit B
Unit C
Q+F
90
10
80
20
70
30
60
40
50
50
40
60
Reno
L
C

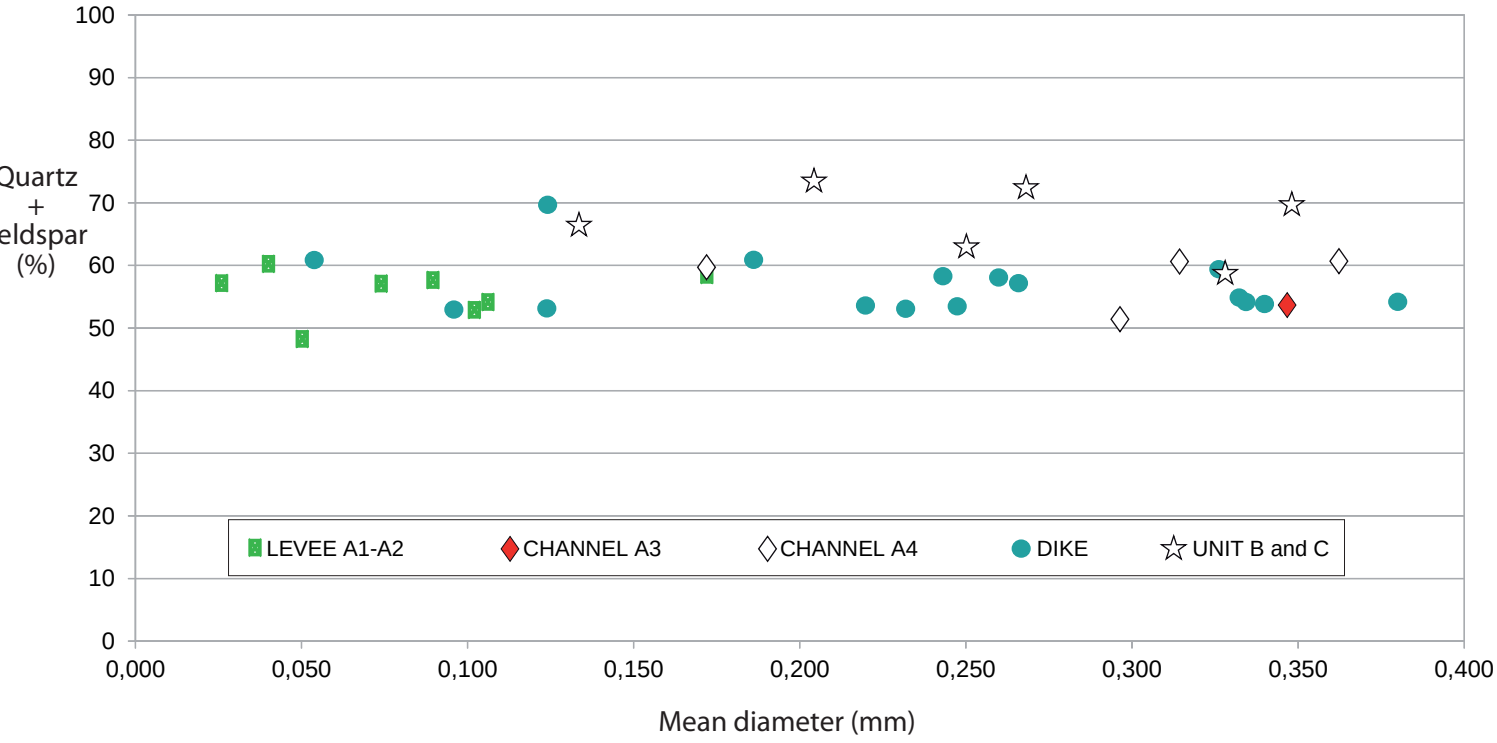
100
90
80
70
60
50
40
30
20
10
0
Quartz + eldspar (%)
0,000
0,050
0,100
0,150
0,200
0,250
0,300
0,350
0,400
Mean diameter (mm)
LEVEE A1-A2
CHANNEL A3
CHANNEL A4
DIKE
UNIT B and C

			RENO RIVER				LEVEE A1-A2								CHANNEL A3	CHANNEL A4				DIKE 3						
		Sample	FR2	FR1	FR3	FR4	SC1 36B	SC1 37B	SC1 38B	SC1 39B	SC1 43B	SC1 44B	SC1 45	SC1 46B	SC1 48	SC1 55	SC1 61	SC1 59	SC1 60	SC1 23	SC1 22	SC1 1	SC1 2	SC1 3	SC1 4	SC1 5
NCE	Q	Quartz single crystal	23,4	27,1	20,6	22,1	28,9	25,9	28,5	31,1	22,3	26,3	30,4	25,3	26,3	26,1	28,9	25,2	22,7	28,0	27,3	25,5	30,7	27,3	21,1	24,2
		Quartz polycrystalline coarse texture	2,2	2,3	3,1	1,4	2,4	1,6	1,6	2,3	9,0	1,9	2,3	2,7	5,0	2,6	3,9	3,8	2,9	10,0	4,8	3,8	4,2	3,8	3,5	4,6
		Quartz polycrystalline fine texture	0,4	1,4	0,8	1,1	0,9	1,9	0,9	1,7	-	3,8	1,0	0,3	1,0	0,6	1,9	2,6	1,3	1,3	1,8	1,0	1,0	1,9	1,6	1,6
		Chert	0,1	0,9	-	0,3	0,3	-	-	0,3	-	0,9	0,3	-	-	-	0,3	0,3	0,3	-	0,3	0,6	-	-	0,6	-
		Quartz in plutonic-gneissic rock fragment	1,8	1,1	-	0,3	0,6	1,6	0,6	0,3	3,0	0,6	-	0,3	2,7	2,6	0,6	0,3	1,0	6,3	0,6	0,3	1,3	-	2,2	0,3
		Quartz in metamorphic rock fragment	0,1	-	-	-	-	0,3	-	0,7	-	0,3	0,7	0,7	-	0,6	1,0	0,2	0,3	-	0,3	-	-	-	0,3	1,0
		Quartz in volcanic rock fragment	-	-	-	-	-	-	-	-	-	-	-	-	-	-	-	-	-	-	-	-	-	-	-	-
		Quartz in clastic rock fragment	2,3	2,3	4,2	3,7	3,3	3,2	1,3	1,3	0,7	2,5	1,3	0,3	0,3	3,9	2,9	1,8	0,3	2,0	5,2	2,9	3,2	1,0	4,1	1,6
	K	K-feldspar single crystal	9,1	9,4	11,3	9,5	8,5	8,1	7,2	10,6	8,7	10,1	10,2	9,0	6,7	11,3	10,7	15,1	7,1	10,3	9,4	12,4	13,3	7,9	12,6	10,5
		K-feldspar in plutonic-gneissic rock fragment	0,6	0,9	1,1	0,9	0,3	-	-	-	0,3	-	1,0	-	0,3	0,3	-	0,2	0,6	0,7	-	0,6	0,3	-	0,9	0,3
		K-feldspar in metamorphic rock fragment	-	-	-	-	-	-	-	-	-	-	-	-	-	-	-	-	-	-	-	-	-	-	-	-
		K-feldspar in volcanic rock fragment	-	-	-	-	-	-	-	-	-	-	-	-	-	-	-	-	-	-	-	-	-	-	-	-
		K-feldspar in clastic rock fragment	0,1	-	0,3	-	0,3	0,3	0,3	0,0	0,3	0,6	0,3	-	-	-	0,3	0,3	0,3	-	-	0,6	-	0,3	-	0,3
	P	Plagioclase single crystal	7,9	4,0	7,9	7,5	9,7	9,7	12,5	7,3	13,3	11,7	9,2	-	10,3	-	8,8	10,1	13,9	9,3	6,4	5,1	6,5	9,5	10,4	5,9
		Plagioclase in plutonic-gneissic rock fragment	-	0,3	0,3	-	0,6	-	0,6	0,3	0,7	0,6	-	8,7	1,0	11,9	0,3	0,5	0,6	1,3	0,6	0,3	0,3	0,6	0,3	1,0
		Plagioclase in metamorphic rock fragment	-	-	-	-	-	-	-	-	-	-	-	0,7	-	0,6	-	-	-	-	-	-	-	0,3	-	-
		Plagioclase in volcanic rock fragment	-	-	-	-	-	-	-	-	-	-	-	-	-	-	-	-	-	-	-	-	-	0,3	-	-
		Plagioclase in clastic rock fragment	0,4	0,6	0,8	0,6	1,5	-	0,3	1,0	-	0,6	-	-	-	-	-	0,5	-	-	0,3	0,3	-	-	0,6	1,6
	L	Metamorphic rock fragment	-	-	-	0,3	-	0,3	-	-	1,7	0,6	-	0,7	2,0	-	-	-	-	0,7	-	-	-	-	-	-
		Volcanic rock fragment	-	-	-	-	-	-	-	-	-	-	-	-	0,7	-	-	-	-	1,7	-	-	-	-	-	-
		Spilite	-	-	-	-	-	-	-	-	0,3	-	-	0,3	-	-	-	-	-	0,7	-	-	-	-	-	-
		Serpentinite	0,4	-	-	0,3	0,3	0,3	-	0,3	-	0,3	0,3	0,3	0,3	-	0,6	-	-	-	0,3	-	0,6	-	-	-
		Clastic lithic Shale	18,3	14,3	18,6	12,4	13,7	16,2	16,3	12,6	10,7	7,3	9,9	10,3	10,7	13,2	14,6	9,9	17,2	1,0	13,6	14,3	11,0	12,4	12,0	12,1
		Clastic lithic Siltstone	6,4	5,7	5,4	7,5	6,1	3,2	4,1	3,6	3,0	4,4	4,6	4,0	3,7	3,9	2,9	4,6	5,8	1,0	2,4	4,1	3,9	2,9	4,1	5,9
	M	Muscovite+Chlorite single crystal	0,1	0,6	1,1	0,6	0,6	1,6	1,9	1,0	0,3	1,3	1,7	4,0	1,7	0,6	-	0,5	0,3	-	0,6	-	0,6	-	1,3	1,6
		Muscovite+Chlorite in rock fragment	0,3	-	-	0,6	0,6	-	-	-	0,3	-	-	0,3	0,7	-	-	0,3	-	0,3	-	-	-	-	0,3	-
		Heavy mineral single crystal (unspecified)	0,3	-	-	1,1	-	-	-	-	-	-	-	-	-	-	-	0,3	0,3	-	-	-	-	-	0,6	-
		Heavy mineral in rock fragment (unspecified)	-	-	-	-	-	-	-	-	-	-	-	-	-	-	-	-	-	-	-	-	-	-	-	-
		Fe-oxide	-	-	-	1,7	-	-	-	-	0,3	-	-	0,7	0,3	-	-	-	-	-	-	-	-	-	-	-
CE	C	Calcite single crystal	11,0	15,7	11,0	16,7	11,2	9,1	11,0	13,9	9,3	9,2	15,8	12,3	14,3	10,6	10,7	10,9	9,4	11,3	10,3	14,0	13,6	15,2	12,0	12,1
		Sparitic limestone	4,5	3,1	3,7	3,2	0,3	2,3	0,9	2,0	6,7	3,8	1,7	9,0	6,0	1,9	1,0	2,2	2,9	4,0	4,2	1,9	1,0	0,6	1,6	0,3
		Silty-arenitic limestone	-	-	-	-	-	0,6	-	-	2,3	-	5,9	0,3	0,3	-	0,3	0,6	0,6	1,3	0,3	1,3	-	-	0,3	0,3
		Mudstone-Wackestone	7,5	6,3	7,6	7,2	7,3	10,0	8,5	7,0	1,7	9,2	-	3,0	3,0	7,1	9,4	7,1	8,4	4,7	7,3	8,9	7,4	10,5	7,3	8,8
		Bioclast (terrigenous)	1,5	2,0	1,1	0,9	1,8	2,6	2,5	2,3	1,0	3,2	3,0	4,7	1,3	1,6	0,6	1,4	2,3	3,7	3,0	1,3	1,0	3,2	2,2	3,6
NCI		Brick and pottery fragments	-	-	-	-	-	-	-	-	-	-	-	-	-	-	-	-	-	-	-	-	-	-	-	-
		Organic material	-	-	-	-	-	1,0	0,9	0,3	-	-	-	-	-	0,3	-	0,2	0,3	-	0,3	-	-	1,0	-	1,6
CI		Bioclast (penecontemporaneous)	-	-	-	-	-	-	-	-	-	-	-	-	-	-	-	0,2	-	-	-	-	-	-	-	-
		Caliche	1,0	2,0	1,1	0,3	-	-	-	-	3,7	-	-	1,7	0,7	-	-	0,3	0,3	-	-	-	-	-	-	-
		Undetermined	-	-	-	-	0,6	-	-	-	0,3	0,6	0,3	0,3	0,7	-	-	0,6	0,6	0,3	0,6	0,6	-	1,3	-	0,7
		Total	100,0	100,0	100,0	100,0	100,0	100,0	100,0	100,0	100,0	100,0	100,0	100,0	100,0	100,0	100,0	100,0	100,0	100,0	100,0	100,0	100,0	100,0	100,0	100,0

			DIKE 4		DIKE 5					DIKE 6	DIKE 7		CORE S3		CORE S2		CORE S10	
		Sample	SC1 6	SC1 7	SC1 41	SC1 49	SC1 19	SC1 20	SC1 21	SC1 32	SC1 34	SC1 33	SC1 52	SC1 53	SC1 51	SC1 50	SC1 28	SC1 26
NCE	Q	Quartz single crystal	21,0	21,9	27,5	21,7	25,9	26,6	34,6	25,7	30,7	26,3	40,0	25,4	31,3	32,9	36,0	31,3
		Quartz polycrystalline coarse texture	4,5	4,6	2,0	3,7	5,2	2,5	1,0	5,3	3,4	4,0	6,0	3,7	6,3	4,3	8,0	6,0
		Quartz polycrystalline fine texture	2,2	2,0	3,6	1,0	0,9	1,6	2,0	0,7	2,8	2,0	1,3	2,1	2,0	2,0	3,3	2,3
		Chert	0,3	-	-	-	-	-	-	0,3	-	-	-	0,3	-	-	1,0	0,5
		Quartz in plutonic-gneissic rock fragment	0,6	0,3	2,3	3,3	1,2	0,6	1,6	2,3	0,3	2,7	3,3	2,1	3,3	2,3	0,3	1,4
		Quartz in metamorphic rock fragment	0,3	0,7	-	0,3	-	0,3	0,7	0,3	0,6	-	-	-	-	-	-	0,3
		Quartz in volcanic rock fragment	-	-	-	-	-	-	-	-	-	-	-	-	0,3	-	-	0,2
		Quartz in clastic rock fragment	2,2	4,2	3,0	2,7	3,1	1,3	2,3	4,0	2,5	2,7	3,3	3,1	-	0,7	0,3	2,3
	K	K-feldspar single crystal	11,5	6,9	8,6	12,7	7,4	9,7	9,8	11,3	12,5	10,0	7,7	12,2	10,0	11,3	12,7	14,8
		K-feldspar in plutonic-gneissic rock fragment	0,6	-	-	0,3	0,6	0,6	-	1,0	-	2,0	1,0	0,6	1,3	1,0	0,3	1,2
		K-feldspar in metamorphic rock fragment	-	-	-	-	-	-	-	-	-	-	-	-	-	-	-	-
		K-feldspar in volcanic rock fragment	-	-	-	-	-	-	-	-	-	-	-	-	-	-	-	-
		K-feldspar in clastic rock fragment	0,3	0,7	-	0,3	-	-	-	-	-	-	-	-	-	-	-	-
	P	Plagioclase single crystal	8,9	12,1	7,6	7,3	9,0	9,4	8,8	6,0	6,0	4,0	10,0	8,3	7,7	12,0	7,3	9,7
		Plagioclase in plutonic-gneissic rock fragment	0,6	-	0,3	0,7	0,3	-	-	1,0	0,3	0,3	1,0	0,6	0,7	0,3	0,3	2,8
		Plagioclase in metamorphic rock fragment	-	-	-	-	-	-	-	-	-	-	-	-	-	-	-	-
		Plagioclase in volcanic rock fragment	-	-	-	-	-	-	-	-	-	-	-	-	-	-	-	-
		Plagioclase in clastic rock fragment	0,6	0,3	-	-	0,6	0,3	-	-	-	-	-	0,6	-	-	-	0,2
	L	Metamorphic rock fragment	0,3	-	-	2,0	-	-	-	1,0	-	3,7	1,7	-	2,3	1,7	1,3	1,2
		Volcanic rock fragment	-	-	-	1,7	-	-	-	1,0	-	0,7	0,3	-	0,7	-	-	-
		Spilite	-	-	-	0,3	-	-	-	0,3	-	-	0,3	-	-	-	0,3	0,2
		Serpentinite	0,6	0,7	-	-	-	0,3	0,3	-	0,3	1,0	-	-	-	-	-	0,2
		Clastic lithic Shale	9,6	12,1	14,9	14,0	9,9	12,9	8,2	8,7	10,3	11,7	2,3	6,7	2,0	5,3	3,3	2,3
		Clastic lithic Siltstone	3,2	2,3	3,0	3,7	4,6	2,2	3,6	3,0	5,6	4,3	1,0	3,7	3,3	1,7	7,3	1,9
	M	Muscovite+Chlorite single crystal	0,3	1,0	1,0	-	0,3	1,9	2,0	2,0	0,6	2,3	-	0,9	0,0	1,0	0,3	-
		Muscovite+Chlorite in rock fragment	0,6	-	-	1,0	-	0,3	0,3	1,0	-	-	0,3	-	0,3	-	0,3	0,5
		Heavy mineral single crystal (unspecified)	0,3	-	0,3	-	0,6	-	-	-	-	-	-	-	-	-	-	-
		Heavy mineral in rock fragment (unspecified)	-	-	-	-	-	-	-	-	-	-	0,3	-	-	-	-	-
		Fe-oxide	-	-	-	0,3	-	-	-	-	-	-	-	-	-	-	0,3	-
CE	C	Calcite single crystal	14,3	14,7	10,3	13,3	13,9	12,5	11,8	12,0	11,9	12,3	13,0	14,7	18,7	15,9	7,3	10,5
		Sparitic limestone	2,2	3,3	6,0	3,0	4,9	0,3	1,0	3,7	3,4	2,7	3,3	2,4	2,3	2,0	2,0	3,2
		Silty-arenitic limestone	0,3	-	-	-	0,3	-	0,3	2,0	0,3	-	-	0,6	2,0	-	-	0,7
		Mudstone-Wackestone	10,2	7,2	7,0	3,3	6,8	11,0	8,2	5,0	6,0	5,0	2,7	8,6	2,0	2,0	6,0	4,7
		Bioclast (terrigenous)	3,2	3,9	2,6	2,7	3,1	4,7	2,6	2,0	0,9	2,3	0,7	2,8	2,3	2,7	1,3	1,1
NCI		Brick and pottery fragments	-	0,0	-	-	-	-	-	-	0,3	-	-	-	-	-	-	-
		Organic material	-	0,3	-	-	0,3	-	-	-	0,3	-	-	0,3	-	0,3	-	0,6
CI		Bioclast (penecontemporaneous)	-	-	-	-	0,3	0,3	0,7	-	-	-	-	-	-	-	-	-
		Caliche	-	-	-	-	-	-	-	-	-	-	0,3	-	0,3	-	-	-
		Undetermined	1,0	1,0	-	0,7	0,6	0,6	0,3	0,3	0,6	-	-	0,3	0,7	0,7	0,3	0,2